Nuclear Inst. and Methods in Physics Research, A 999 (2021) 165230

Contents lists available at ScienceDirect

Nuclear Inst. and Methods in Physics Research, A

journal homepage: www.elsevier.com/locate/nima

Quantitative analysis and benchmarking of positional accuracies of neutron strain scanners

R.S. Ramadhan [a,*], S. Cabeza [a], T. Pirling [a], S. Kabra [b], M. Hofmann [c], J. Rebelo Kornmeier [c], A.M. Venter [d], D. Marais [d]

[a] Institut Laue-Langevin, 71 Avenue des Martyrs, 38000 Grenoble, France
[b] STFC-Rutherford Appleton Laboratory, ISIS Facility, Harwell, OX11 0QX, United Kingdom
[c] Heinz Maier-Leibnitz Zentrum, TU München, Lichtenbergstr. 1, D-85747, Garching, Germany
[d] Necsa SOC Limited, PO Box 582, Pretoria, 0001, South Africa

ARTICLE INFO

Keywords:
Neutron strain scanners
Neutron quality label
Neutron diffraction
Positional accuracy
Internal strain analysis

ABSTRACT

Positional accuracy is an important parameter in residual stress investigations with neutron diffraction, considering that precise measurements of strains at the same localised position along a number of sample orientations are required, including investigations of complete complex shaped engineering components. This study reports the development of a standardised approach for quantitative analysis of positional accuracy on neutron strain scanners that builds on previous campaigns. The approach uses standardised sample sets with specific geometries that enable quantitative assessment of instrumental and sample alignment procedures and associated accuracies. This method has been implemented on four participating instruments: ENGIN-X (United Kingdom), MPISI (South Africa), SALSA (France) and STRESS-SPEC (Germany), to render results representative of monochromatic and time-of-flight strain scanners. The benchmarking results show comparable performance between the instruments with positional accuracies around 100 μm readily achieved. This standardised approach confirms the high positional precision attainable for non-destructive stress determination, to unequivocally benefit utilisation by academia and industry alike. It is envisaged that this common calibration protocol and reporting template that conforms to the newly developed Neutron Quality Label for Internal Stress Characterisation be adopted by other facilities to facilitate expansion of the supportive network.

1. Introduction

The neutron diffraction-based method for internal strain analysis of polycrystalline materials has specific advantages, amongst others the non-destructive depth-resolved determination of the complete stress tensor within engineering components. The value addition of the technique has been proven to be beneficial in the research and development of products in vital sectors such as aerospace, transport, energy, and manufacturing [1–9]. Technical development and standardisation of neutron diffraction procedures for residual stress determination have been performed through previous projects including the Versailles Project on Advanced Materials and Standards: Technical Working Area 20 (VAMAS TWA20) and the Residual Stress Standard using Neutron Diffraction (RESTAND) program [10,11]. These documents, in conjunction with the ISO 21432:2019 standard [12] serve as the general guideline for residual stress determination using neutron diffraction.

Due to the progress in new component manufacturing techniques such as additive manufacturing, novel welding methods and surface processing, the utilisation of neutron diffraction stress determination and the complexity of investigations are becoming more demanding. At the same time, the pool of neutron strain scanning instruments internationally have largely remained constant over the years [13], with many of the instruments at the Large Scale Research Infrastructures (LSRI) being heavily oversubscribed. To efficiently expand the support network of available instruments and to instill confidence with users in the unequivocal utilisation of instruments at different institutes collaboratively, notwithstanding inherent instrumental differences between neutron strain scanners, interchangeability of performance between instruments need to be well characterised.

Therefore, to advance from the previous standardisation initiatives, a Neutron Quality Label (NQL) is proposed as a quality standard for the verification of neutron strain scanner performances within the international neutron landscape. This label is attainable by the approval of the NQL participating members following a demonstration of similar investigations on the common calibration samples and reporting of results in the standardised format [14].

* Corresponding author.
E-mail address: ramadhan@ill.fr (R.S. Ramadhan).

https://doi.org/10.1016/j.nima.2021.165230
Received 27 November 2020; Received in revised form 8 March 2021; Accepted 8 March 2021
Available online 17 March 2021

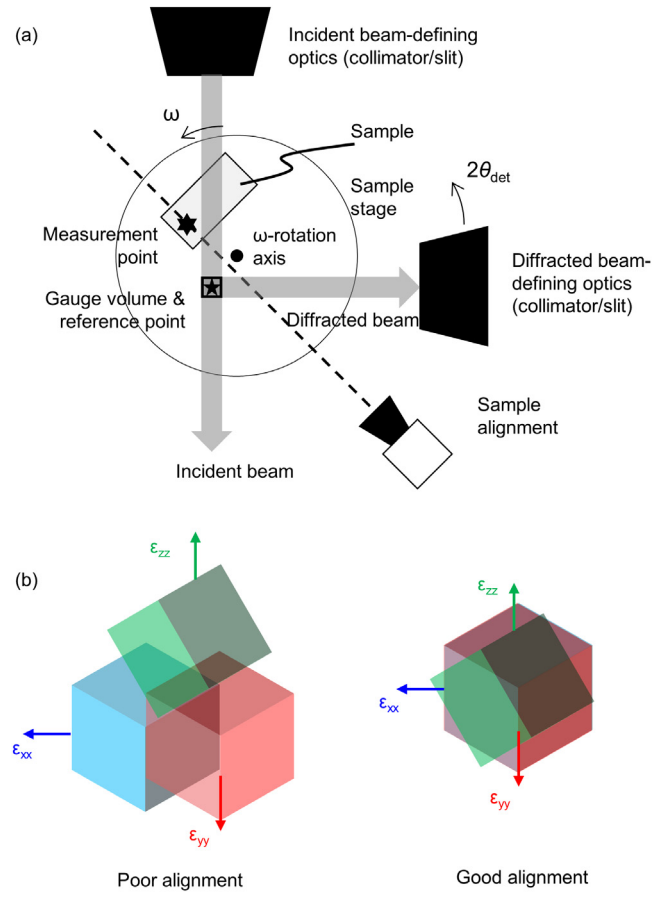

Fig. 1. (a) Top view illustration of the main components and important features of a neutron strain scanner instrument magnifying alignment errors; (b) Illustration of the effect of instrumental and sample misalignment against perfect alignment.

The objective of this study is to report the project design of this initiative which includes calibration samples, methods descriptions and inter-comparative benchmarking investigations on four participating neutron strain scanner instruments representing both monochromatic and time-of-flight (TOF) configurations, as well as lessons learned [15].

2. Methods & materials

2.1. Positional accuracy

Fig. 1(a) illustrates the main components and important features associated with a neutron strain scanner. The important features are: (a) the centre of ω-rotation of the instrument which is a fixed vertical axis around which sample rotation and the measurement geometry is performed; (b) the anticipated measurement point, as determined using the optical or mechanical alignment system on the instrument; (c) the "reference point", which according to ISO 21432-2019 [12] is the centre of the instrumental gauge volume, the gauge volume (GV) as it is generated by the beam optics as intersection of the incident/primary- and diffracted/secondary beam. An essential requirement is to have the reference point coincident with the instrument centre of ω-rotation within an accuracy of 10% of the neutron gauge volume width. This is to ensure that the measured local lattice spacing (that is directly convertible to elastic strain) information along different directional orientations (as required for tri-axial stress calculation), is measured from the same localised volume within the sample.

The sample position is aligned to the reference point and the centre of ω-rotation by using a sample alignment system, which could be either optical, mechanical, or by means of the entry scan method which entails scanning the gauge volume incrementally across the surface of the sample and fitting an analytical model to the measured intensity profile (entry curve) [16]. Any inaccuracy in relative positioning will introduce offsets in the position of the GV within which the strains are being determined. The consequence of deliberate misalignment between the various parameters on the measurement volume is illustrated in Fig. 1(b). This can lead to inaccurate stress determination, especially in samples with steep stress gradients as the calculation requires a number of different strain-orientation measurements at the same location. While instrumental (motor) positioning errors are inherent to any mechanical system and thus unavoidable, instrument setup characterisation is imperative to quantify the contribution of such uncertainties to the systematic positional accuracy.

In this study, methods were developed that facilitate evaluation of the main contributing parameters to the positional accuracies of neutron strain scanners. Within the assumption that the mechanical axes of the sample manipulation system are perfectly aligned to the instrument centre of ω-rotation, the key objectives of this study were:

- To evaluate the reference point positioning accuracy with respect to the instrument centre of ω-rotation.
- To study the effect that different detector angular positions ($2\theta_{det}$) has on the viewed reference point in instruments with single detectors (normally constant wavelength instruments) and to quantify the correlation between the reference points viewed by instruments equipped with multiple detectors (normally time-of-flight instruments).
- To quantify the precision of devices employed as external alignment aids, such as cameras and theodolites, in setting up and aligning samples to the instrument reference point.
- To quantify the accuracy and robustness of entry curve analysis software used by the participating instruments.

2.2. Participating instruments

The participating neutron strain scanners in this study are three monochromatic instruments: SALSA, ILL (France), STRESS-SPEC, MLZ (Germany), and MPISI, Necsa (South Africa) [17–19], and one time-of-flight instrument: ENGIN-X, ISIS (UK) [20]. In this document, the participating strain scanners are referred to as Instrument 1 to 4 without any particular order. The incident wavelength λ on all monochromatic instruments lay in the range 1.64–1.67 Å, produced from Si monochromators, as well as $\lambda = 1.35$ Å using a Ge monochromator. The wavelength range on ENGIN-X was 0.6–4.5 Å. Each instrument is equipped with sample positional stages that have translation accuracies better than ±20 μm attainable with high precision mechanics integrated with direct probing positional encoders. Theodolites and/or telecentric camera systems are used as sample alignment systems. These generally have an accuracy better than 100 μm. Different combinations of slits and radial collimators for incident beam and/or detector (diffracted beam) optics were used in these investigations to evaluate their impact in conjunction with different gauge volume sizes and spatial definitions.

2.3. Test samples

The standardised sample set comprises: (a) Calibration Foil & pin sample; (b) 5-wall sample, and; (c) Tube sample, as shown in Fig. 2. The 5-wall and Tube samples were manufactured to general tolerance specification ISO 2768-f. The manufactured geometries and sample features were measured using a coordinate measurement machine (CMM) at the Material Science Support Laboratory of the ILL. The measurements utilised a Mitutoyo Euro-C776 APEX machine coupled with SP600 scanning probe system (resolution of 0.1 μm) in conjunction with MCOSMOS V4 software. Three identical sample sets were manufactured and shared between the participating facilities.

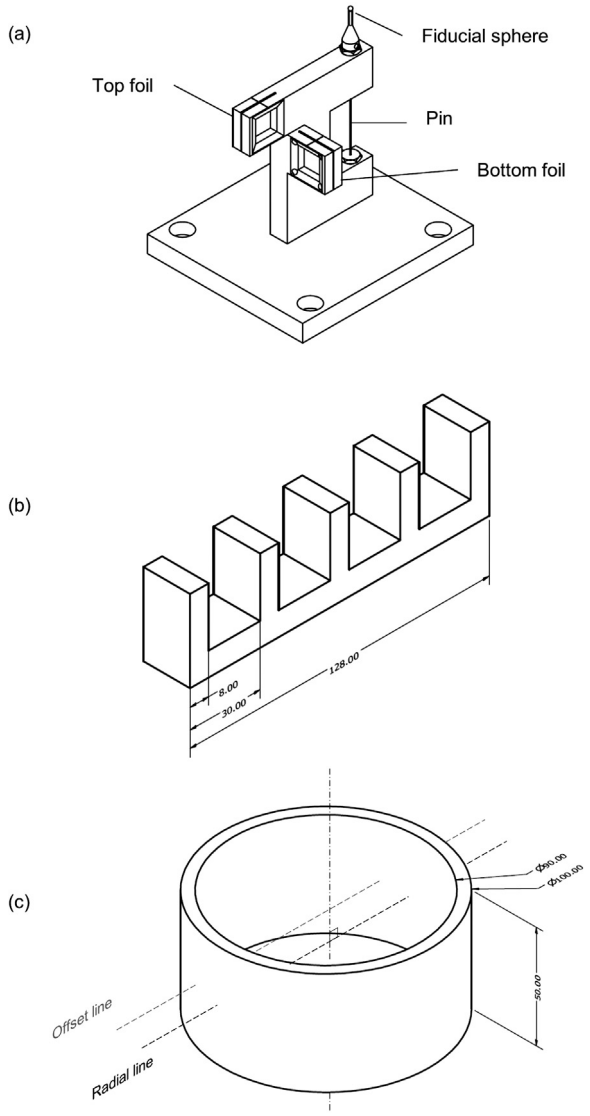

Fig. 2. Calibration samples: (a) Foil and pin sample instrument alignment as well as determination of alignment inaccuracies; (b) 5-wall sample, and; (c) Tube sample, used for verifying precision of sample alignment. Main features are indicated.

The Foil & pin sample contains two thin foils, respectively mounted perpendicular to each other, as well as a vertical pin with a fiducial sphere on the one end, all mounted on an sturdy frame as shown in Fig. 2(a). The foils are at different heights, therefore named top and bottom foil. These samples enable: (a) Alignment of the beam-defining optics; (b) Determination of the reference point position with respect to the instrument's centre of ω-rotation; (c) Determination of the accuracy of the goniometer axes alignment to the instrument centre of rotation. The fiducial sphere serves as an additional reference to assist with the alignment of the pin to the reference point (if required). The orthogonal foil configuration allows investigations along two different scattering geometries, i.e. transmission and reflection, by x, y, z repositioning without sample rotations (ω-angle). The foils and pin materials are exchangeable and can have different thickness/diameter. For this study, the material of the pin, sphere and foils were all ferritic steel. The pin and fiducial sphere had a diameter of 1 mm and the foils were 0.3 mm thick.

The austenitic stainless steel 5-Wall sample consists of five identical vertical walls each 8 mm in thickness and equivalently spaced as depicted in Fig. 2(b). This structure allows repeated investigations of identical and relatively simple-to-align flat geometries using a single sample and is therefore efficient for studying the reproducibility/precision of sample alignment routines and instrument mechanics. In addition, it was used to study the accuracy of entry curve analysis software used to determine the position of both perpendicular as well as inclined surfaces (see Section 3.3).

The austenitic stainless steel Tube sample has an outer diameter of 100 mm and wall thickness of 5 mm as presented in Fig. 2(c). This sample facilitates studying the robustness of the entry curve analysis software in determining the sample surface positions for a complex gauge volume immersion geometry due to curved surfaces. Investigations were performed along two lines as shown in Fig. 2(c): (1) 'radial line', being a line along the tube diameter (with the tube axis vertical); (2) 'offset line' being a line parallel to the radial line, but horizontally offset to not be coincident with the tube diameter. The latter results in a relatively complex gauge volume sample surface intersection geometry. In addition, a measurement was also conducted with the tube axis in a horizontal orientation and corresponds to a typical setup that is routinely used for the measurement of the axial strain component.

3. Experimental

The instrument axis of rotation needs to be accurately determined in advance by employing for instance a dial gauge or other optical methods. The incident and diffracted beam-defining optics, as well as the external optical alignment instrumentation must then be aligned to be coincident to this reference axis to within 10 μm. The reference axis, in conjunction with the beam mid-height defines the reference point for the measurement geometry.

3.1. Pin scan

A Pin scan was performed to investigate the correlation between detector angular positions ($2\theta_{\mathrm{det}}$) and the reference point position. This was done by systematically scanning the Pin across the diffracted beam in the direction of the incident beam while keeping the ω-angle fixed as shown in Fig. 3(a). On two of the instruments these investigations were performed at different $2\theta_{\mathrm{det}}$ positions which correspond to different *hkl* reflections of the material. When using slits as the diffracted beam-defining optics they were re-aligned at each $2\theta_{\mathrm{det}}$ position (*hkl* reflection). This ensures the reproducibility of measurement locations between the respective investigations. As an extension of this test a measurement was performed by employing a radial collimator as the diffracted beam-defining optics without re-alignment after $2\theta_{\mathrm{det}}$ repositioning. This provides information on the geometrical effect of reference point displacement. The nominal gauge volume size (nominal, i.e., determined by the openings of the beam-defining optics without considering beam divergence) was 1.0 × 1.0 × 10.0 mm^3 (primary width × secondary width × height) on two of the instruments and 0.6 × 0.6 × 2.0 mm^3 for the other. These investigations were not performed on the TOF instrument since its detectors are at fixed angular positions. A summary of the experimental conditions is given in Table 1.

3.2. Foil scan

So-called foil scans were performed to determine the position of the reference point with respect to the centre of ω-rotation. This was done by scanning the metal foils, much thinner than the dimensions of the gauge volume, across the gauge volume in reflection and transmission geometry as illustrated in Fig. 3(b). Investigations were performed for two different *hkl* reflections, respectively observed at two different diffraction angles whilst keeping the wavelength constant. For each $2\theta_{\mathrm{det}}$ position the measurements were carried out at a minimum of three orthogonal ω-angles. Note that similarly to the Pin investigations, the diffracted beam aperture alignment was performed at a single detector angular position on one of the constant wavelength instruments, whilst

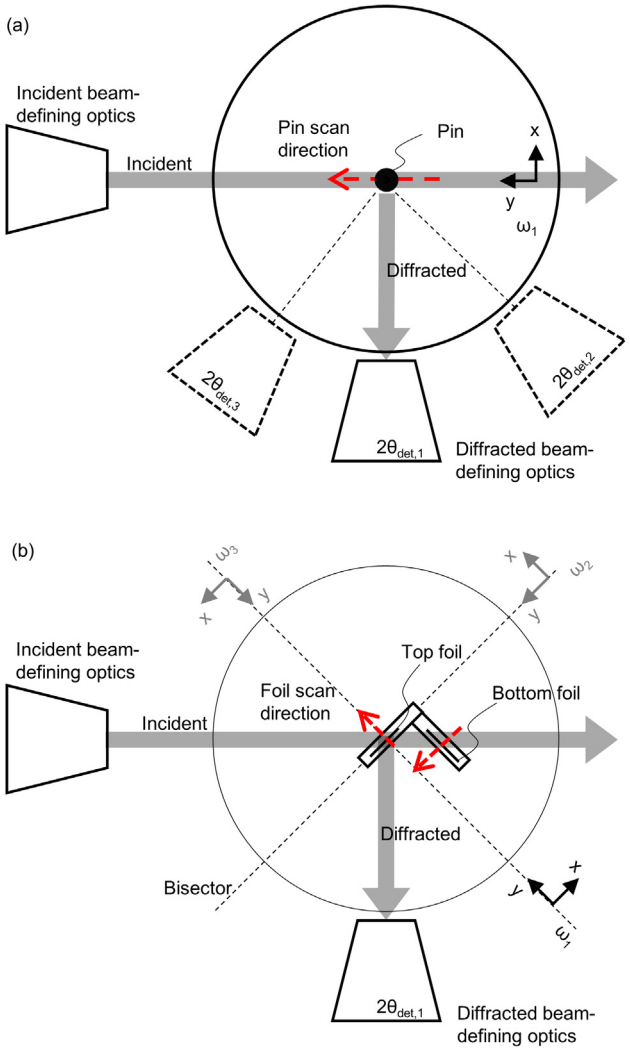

Fig. 3. (a) Top view illustration of the pin scan investigation, performed at different detector angular positions; (b) Illustration of the investigations on the top and bottom foils. The respective bisector angles for the two measurement geometries (transmission and reflection) are shown by the dotted lines. The orientation shown corresponds to measurement in transmission and reflection geometry respectively for top and bottom foil.

Table 1
Summary of the pin scan exercises on the participating neutron strain scanners.

Inst.	*hkl*	$2\theta_{det}$ (°)	Beam optics type[a]	Alignment at $2\theta_{det}$ = (°)
1	Fe(211)	93.5	Collimator (I) –Collimator (D)	93.5
	Fe(110)	49.8		
2	Fe(211)	92	Slit (I)–Collimator (D)	92
	Fe(200)	72	Slit (I)–Slit (D)	92, 72, 49
	Fe(110)	49		
3	Fe(211)	90	Slit (I)–Slit (D)	90, 50, 105
	Fe(110)	50		
	Fe(220)	105		

[a](I) – Incident beam; (D) – Diffracted beam.

on the others, re-alignment was performed at each detector position. The summary of the foil scan exercises on the participating instruments is given in Table 2. Different $2\theta_{det}$ values for the same reflection on Instrument 1 is due to different incident beam wavelengths used.

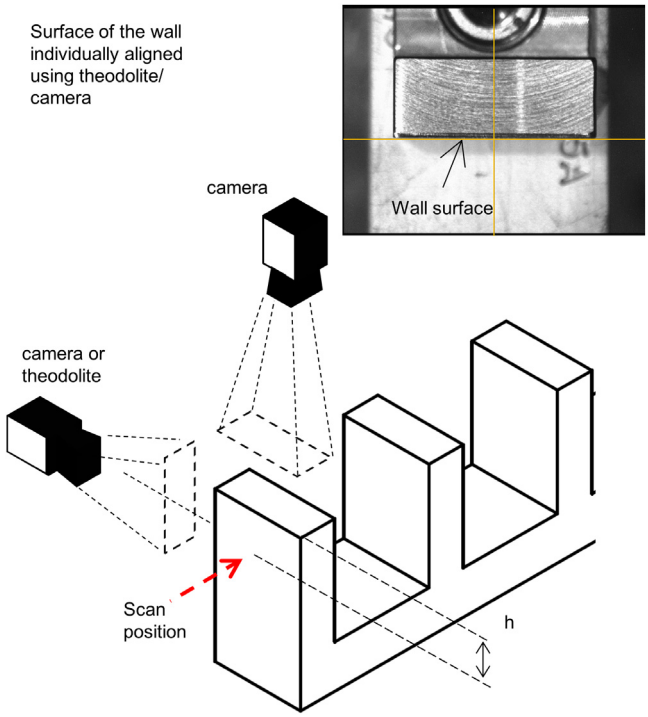

Fig. 4. Wall scan to determine the precision of sample alignment using an optical system. The inset shows an example of the field-of-view of a telecentric camera used in one of the instruments.

3.3. Wall scan

A wall scan is a complete incremental scan of the neutron gauge volume through the wall thickness. In this study, scans were performed on the walls of the 5-Wall sample, as well as on the Tube sample. Results from the wall scans were used to evaluate the correlation between sample alignment procedures using both optical and the neutron entry scan method, the latter in conjunction with corresponding software.

Scans on the 5-Wall sample were used to determine the precision of the optical sample alignment systems (i.e. theodolite or camera as implemented on different instruments) compared to the neutron measurements as shown in Fig. 4. The standard deviation of the offsets was then used to determine the precision of sample alignment. Scans on the 5-Wall sample and the Tube sample were used to quantify the accuracy of the entry curve analysis software in determining sample surface positions. The analysis software analytically fits parameters in the entry curve models to the integrated peak intensity data using a least squares solution. From these results wall thicknesses were determined and compared against the CMM measurements.

To quantify the accuracy of the software in determining the position of flat surfaces perpendicular (vertical) to the horizontal diffraction plane ($\chi = 0°$), scans were performed on the 5-Wall sample as shown in Fig. 5(a). A digital inclinometer with an accuracy of 0.1° was used to align the sample to the absolute horizontal plane. Scans were also performed on the wall surfaces of the 5-Wall sample with tilts introduced in order to study the robustness of the software in detecting inclined surfaces, as can be encountered with some real-world engineering components. Using the digital inclinometer, the introduced tilts were $\chi = 2°$ and 10° as shown in Fig. 5(b) and (c) respectively. Entry scans were also performed on the Tube sample to study the robustness of the software in determining the position of curved surfaces, again representative of some real component characterisation. Scans were performed along the radial line and the offset line, with the axis of the tube vertical as shown in Fig. 5(d), as well as with the axis of the tube horizontal as shown in Fig. 5(e). Details of the measurements performed on the participating instrument are provided in Table 3.

Table 2
Summary of the foil scan exercises on the participating neutron strain scanners.

Inst.	*hkl*	$2\theta_{det}$ (°)	ω-angle (°)	NGV size	Beam optics type[a]	Alignment at $2\theta_{det}$ = (°)
1	Fe(211)	89	−45.5 44.5 134.5	0.6 × 0.6 × 2.0 2.0 × 2.0 × 2.0	Collimator (I)–Collimator (D)	89
	Fe(110)	48	−66 24 114	2.0 × 2.0 × 2.0		
2	Fe(211)	92	136 46	1.0 × 1.0 × 10.0	Slit (I)–Collimator (D) Slit (I)–Slit (D)	92 92, 72
	Fe(200)	72	−44 −54 36 126			
3	Fe(211)	90	135 45	1.0 × 1.0 × 10.0	Slit (I)–Slit (D)	90, 50
	Fe(110)	50	−45 −135 25 115 −155			
4	Multiple	90/−90	135 45 −45	2.0 × 2.0 × 10.0	Slit (I)–Collimator (D)	90, −90

[a](I) – Incident beam; (D) – Diffracted beam.

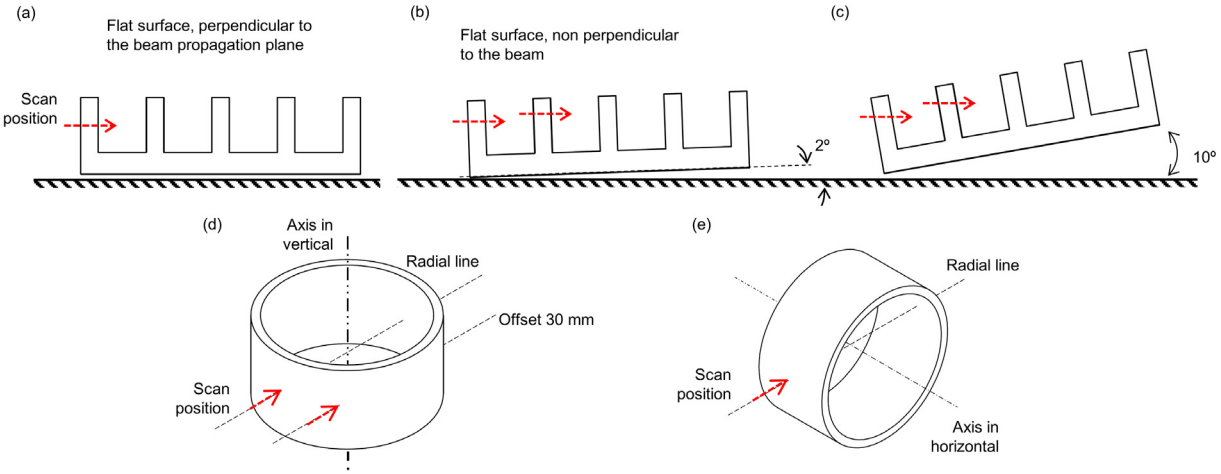

Fig. 5. Wall scan of 5-wall sample with (a) surfaces perpendicular to the diffraction plane; scans with tilt (inclined) angle (b) χ = 2° and (c) χ = 10° from the diffraction plane; Wall scan of the Tube sample (d) with tube axis in vertical, along radial line and offset line; (e) with tube axis in horizontal, along radial line.

3.4. Data analysis

For the pin and foil scans, the diffracted intensity curves were fit with a Gaussian function to determine the measured position of the reference point relative to the pin/foil alignment position. An example is given in Fig. 6. By comparing the alignment position and the measured position of the pin/foil, the offset can be determined.

The intersection of the offsets from the two foil measurements at a particular ω-angle represents the sample position relative to the reference point (cross symbols in Fig. 7, for measurements at ω = 134.5°, 44.5°, and −45.5°). The coordinates of the sample positions in the sample stage coordinate system *xy* were then transformed by an angle ω to the instrument reference coordinate system *XY*. Using results from a minimum of three ω-angles, a circle can be fit where the centroid is the ω-rotation axis position (green dot symbol in Fig. 7) relative to the reference point (yellow star symbol). The radius of the fit circle represents the uncertainty of positioning/alignment of the two foils, i.e., using the optical alignment devices, the foil positions could be determined anywhere along the 0.3 mm thickness of the foil and might not be consistent for the two foils. This analysis can either be carried out mathematically or with the aid of a graphical analysis tool [21].

For wall scans, the intensity curves were fit using entry curve analysis software to determine the measured surface position relative to the alignment position, and measured sample thickness relative to the CMM measurement. Fig. 8 shows examples of intensity curve fits for reflection and transmission geometries. A number of different entry curve analysis software programs (developed by instrument scientists) largely based on the models presented by Brand and Prask [16] exist. The models allow input of fit-parameters such as incident and diffracted beam widths and profiles, beam attenuation by the sample material, offset of sample position to the reference point and sample thickness for a more accurate fit. For example, beam dimensions can be pre-determined from a pin scan type measurement and deconvolution. The programs used by the participating laboratories of this study were: “Align” (V. Luzin, personal communication, September 2019) and “ScanManipulator” [22] which is extensively used for flat surfaces perpendicular (vertical) to the horizontal diffraction plane and “FIT Pseudo Strain” (T. Pirling personal communication, September 2019),

Table 3
Summary of the wall scan exercises from the participating neutron strain scanners on the 5-wall sample, as well as the Tube. Nominal gauge volume (NGV) size is primary width × secondary width × primary height. Secondary beam maximally open vertically.

Inst.	Wall scan type	NGV size (mm^3)	Details
1	Flat surface, perpendicular to beam plane	0.6 × 2.0 × 2.0 2.0 × 2.0 × 2.0	Fe(220)
	Curved surface, radial line, tube axis in vertical	0.6 × 0.6 × 2.0	Fe(220)
2	Flat surface, perpendicular to beam plane	1.0 × 1.0 × 8.0	Fe(220), Fe(311)
	Flat surface, inclined to beam plane	1.0 × 1.0 × 2.0	Fe(220), χ = 2°, 10°
	Curved surface, radial line, axis in vertical	1.0 × 1.0 × 2.0	Fe(220)
	Curved surface, offset line, axis in vertical	1.0 × 1.0 × 2.0	Fe(220), offset 30 mm
	Curved surface, radial line, axis in horizontal	1.0 × 1.0 × 2.0	Fe(220)
3	Flat surface, perpendicular to beam plane	1.0 × 1.0 × 10.0	Fe(220), Fe(200)
	Flat surface, inclined to beam plane	1.0 × 1.0 × 10.0	Fe(220), χ = 2°, 10°
	Curved surface, radial line, axis in vertical	1.0 × 1.0 × 10.0	Fe(220)
	Curved surface, offset line, axis in vertical	1.0 × 1.0 × 10.0	Fe(220)
	Curved surface, radial line, axis in horizontal	1.0 × 1.0 × 10.0	Fe(220)
4	Flat surface, perpendicular to beam plane	2.0 × 2.0 × 10.0 1.0 × 1.0 × 15.0	Multiple *hkl*-planes
	Curved surface, radial line, axis in vertical	2.0 × 2.0 × 10.0	Multiple *hkl*-planes
	Curved surface, offset line, axis in vertical	1.0 × 1.0 × 15.0	Multiple *hkl*-planes, offset 30 mm

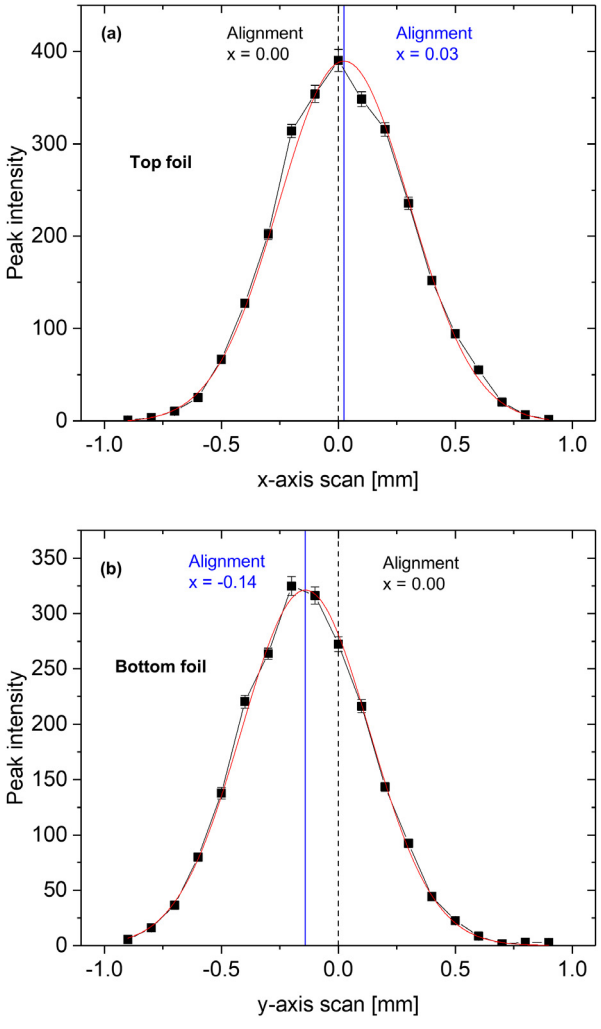

Fig. 6. Intensity profiles from the foil scans, fitted with a Gaussian function, taken from measurements for the Fe(211) measured in (a) transmission and (b) reflection geometry respectively for top and bottom foil. The positions determined from neutron beam measurements were $x = 0.03$ and $y = -0.14$ (in mm) for the top and bottom foils, and the optical alignment position were $x, y = 0, 0$ (in mm), for the top and bottom foil, respectively.

which takes into account sample geometry for the analysis of non-flat surfaces.

4. Result and discussion

4.1. Quantification of reference point position

Table 4 presents the measured reference point positions at different $2\theta_{det}$ positions, determined from the pin scan exercises along the incident beam. Using a radial collimator as the diffracted beam-defining optics, the results reveal that changing $2\theta_{det}$ without re-alignment of the diffracted beam-defining optics leads to significant displacement of the reference point position viewed by the neutron beam in relation to the instrumental reference point. On Instrument 1, aligned at $2\theta_{det} = 93.5°$, repositioning at $2\theta_{det} = 49.5°$ without diffracted beam-defining optics re-alignment, a displacement of ~80 μm is observed in the reference point position (Table 4 No. 1 & 2). For the first set of measurements on Instrument 2, aligned at $2\theta_{det} = 92°$, repositioning at $2\theta_{det} = 72°$ and 49° without diffracted beam-defining optics re-alignment, the reference position was displaced by ~210 μm and ~270 μm respectively (Table 4 No. 3 to 5). For the second set of measurements on Instrument 2, using slits as the diffracted beam-defining optics, with individual diffracted beam-defining optics alignments performed at $2\theta_{det} = 92°$, 72°, and 49°, the reference point positions are reproducible within ~50 μm (Table 4 No. 6 to 8). On Instrument 3, also using slits as the diffracted beam-defining optics with individual re-alignment at each detector angular position, the reference point positions are reproducible within 60 μm (Table 4 No. 9 to 11).

Applying the analysis method described in Section 3.4 to the foil scan results as function of ω-rotation, Figs. 9 to 11 show the correspondence between the reference point positions and the centre of ω-rotation, presented in the sample stage coordinate system, *xy*. On Instrument 1, measured using a radial collimators aligned at $2\theta_{det} = 89°$, the misalignments were ~20 μm and ~100 μm respectively for measurements using gauge volume widths of 0.6 mm and 2 mm, Fig. 9(a) and (b). Scans performed at $2\theta_{det} = 48°$ with a gauge volume width of 2 mm, without re-alignment of the diffracted beam-defining optics, lead to ~600 μm misalignment (displacement of ~700 μm from the initial position at $2\theta_{det} = 89°$) as shown in Fig. 9(b). A similar observation, Fig. 10(a), was found on Instrument 2 aligned at $2\theta_{det} = 92°$ with a gauge volume width of 1 mm, established with a radial collimator for the diffracted beam, leading to misalignments of ~60 μm and ~250 μm respectively at detector angular positions $2\theta_{det} = 92°$ and 72°.

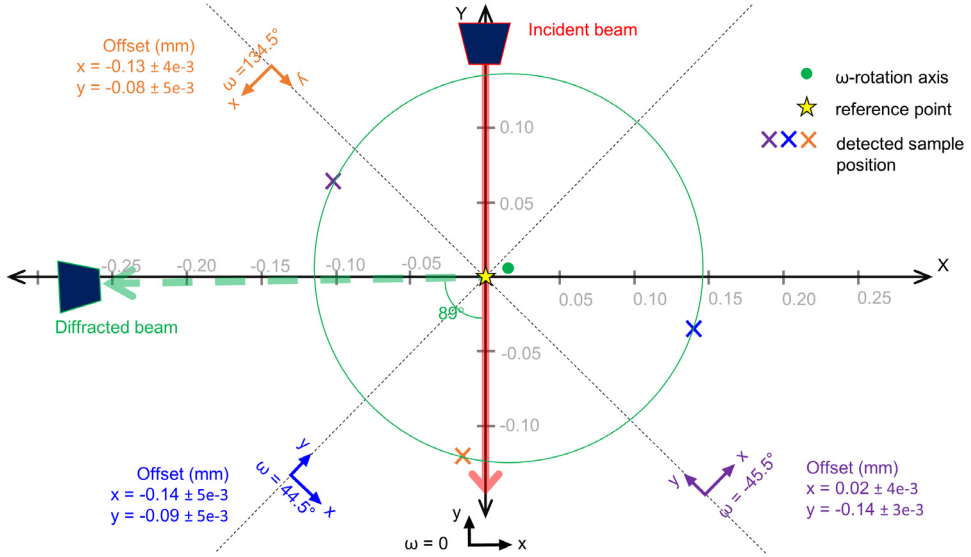

Fig. 7. Top view of an instrument, illustrating of the analysis to determine the reference position relative to the measured sample position. The measurement of sample position by foil scans (cross symbols) at a minimum of three ω-angles allowed the determination of the centre of ω-rotation (green dot symbol) relative to reference position (yellow star symbol).

Table 4
Measured reference point position for different detector $2\theta_{det}$ positions, from pin scan exercises.

Details	No	$2\theta_{det}$(°)	Reference point position (unit in mm)		
			Theoretical	Measured	Standard error
Instrument 1	1	93.5	0.00	0.02	0.01
alignment at $2\theta_{det}$ = 93.5°	2	49.5	0.00	0.10	0.01
Instrument 2	3	92	0.00	0.03	0.00
alignment at $2\theta_{det}$= 92° only	4	72	0.00	−0.18	0.01
	5	49	0.00	−0.24	0.01
Instrument 2	6	92	0.00	−0.29	0.00
alignment at all $2\theta_{det}$ positions	7	72	0.00	−0.25	0.01
	8	49	0.00	−0.26	0.01
Instrument 3	9	90	0.00	0.03	0.01
alignment at all $2\theta_{det}$	10	50	0.00	0.09	0.01
	11	105	0.00	0.05	0.02

Fig. 10(b) and (c) shows results from measurements using slits to shape both the incident and the diffracted beams on Instruments 2 and 3. Here diffracted beam-defining optics alignment was performed at each $2\theta_{det}$. It is obvious that the misalignment, ~20 μm, at different detector angular positions was significantly reduced. Fig. 11 shows the results from the TOF instrument equipped with multiple detectors. Using a gauge volume width of 2 mm, the misalignments were ~30 μm and ~120 μm for the two detector banks and ~100 μm between the two banks. This still represents an accuracy within 5% of the gauge volume width.

The reference point positions quantified above and their relation with the centre of ω-rotation on each instrument is only valid for the specific setup applied during the experiment and the current state of the instrument's mechanics. These results provide the typical reproducibility for each instrument, as long as similar setup and alignment procedures are followed. It is important to note that in Figs. 9 to 11, slight displacements of the reference point position across the incident beam exist in the case of multiple detector angular positions or banks. These are not a real gauge volume displacement, but rather represent the uncertainty of the foil scan method, which was observed to be below 3% of the gauge volume width. This uncertainty of was further confirmed by repeat measurements with the same setup, which showed similar consistencies in the reference point determination.

For the three monochromatic instruments that are all equipped with single position sensitive detectors, it is obvious that the reference point position could incidentally become displaced when the detector angular position changes (pin scan result in Table 4 No. 1 to 5, also foil scan results in Fig. 9(b) and Fig. 10(a)). For example, the displacement was observed up to 700 μm for a 41° $2\theta_{det}$ re-positioning for a gauge volume width of 2 mm, representing a shift of 35% of the gauge volume width. Therefore, this effect must be accounted for in sample investigations that requires measurements at multiple detector positions. Since these displacements were even observed when using radial collimators, which should be independent of the scattering angle [23], it is proposed that this effect results from non-concentricity between the rotation axes of the $2\theta_{det}$ and ω stages on the instrument and/or other contributions related to the mechanical components which drive and guide the movements of the diffracted beam-defining optics/detector support. Nevertheless, this effect can be corrected for by alignment of the beam-defining optics. Results from the pin scan shown in Table 4 No. 6 to 11 and the foil scan results in Fig. 10(b) and (c) indicate that the reproducibility of the alignment procedures of the diffracted beam-defining optics can be within 50 μm precision. Furthermore, the results also showed that the use of slits vs. collimators does not impact the accuracy of the instrument alignment.

4.2. Precision of sample alignment using an optical system

The precision of sample alignment procedures using the instrument specific optical systems was assessed by determining the edges of the

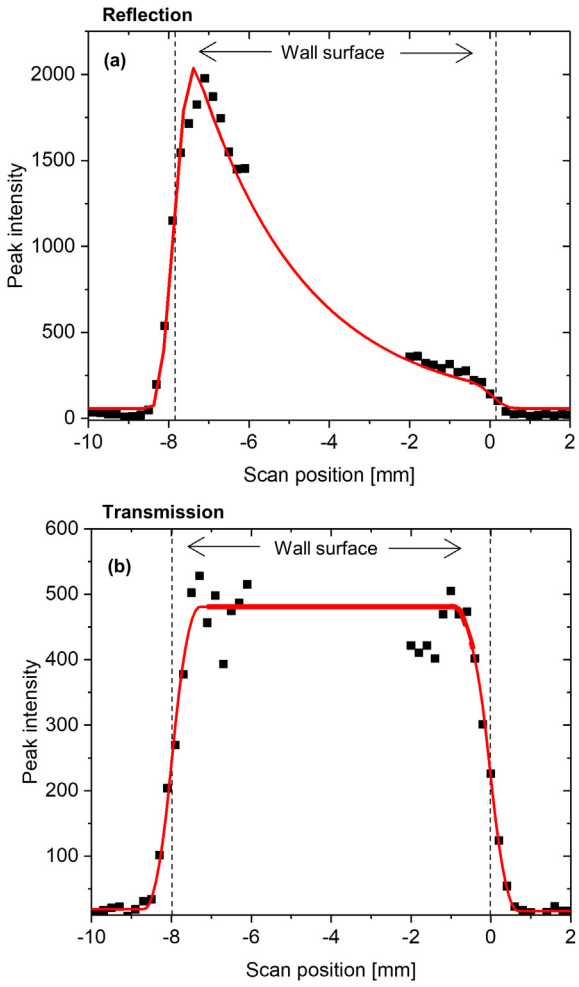

Fig. 8. Example of neutron beam entry curves respectively taken in (a) reflection and (b) transmission geometries from one of the walls of the 5-wall sample.

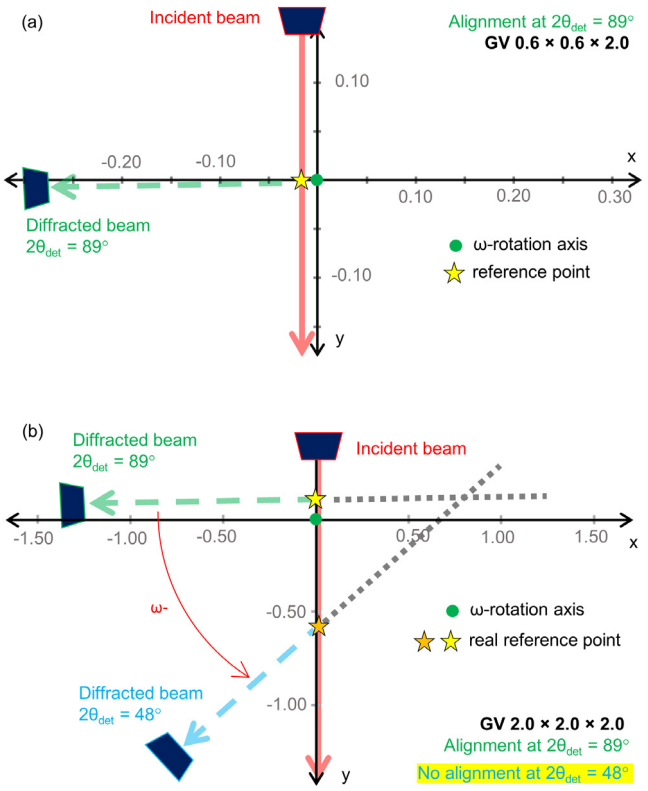

Fig. 9. Reference point relative to the centre of ω-rotation on Instrument 1, scales in mm. (a) Using NGV of 0.6 × 0.6 × 2.0 mm^3 and diffracted beam-defining optics alignment at $2\theta_{det}$ = 89°, it was found that the reference point was misaligned by about 20 μm from the ω-rotation axis; (b) Changing the detector angular position from 89° to 48° without following it up by a diffracted beam-defining optics re-alignment caused a shift in the reference point by 700 μm. Measurements were performed using a NGV of 2.0 × 2.0 × 2.0 mm^3.

5-wall sample using the cameras or theodolites, and comparing it with results obtained from neutron measurements. The standard deviation of the offsets represents the alignment precision, i.e. the ability in repeatedly arriving to the same position, in this case simulated by the surface positions of the various walls. The summary of the results from this exercise is presented in Table 5.

The sample alignment precision between the different instruments was between 50–120 μm and independent of the measurement setup ($2\theta_{det}$ which determines gauge volume shape, gauge volume size, and measurement geometry). Thus with the assessed optical systems, sample surface alignments were achieved within precision of ~100 μm, being in the same order of accuracy of the reference point position studied in Section 4.1, and lay within the stated specification of the cameras and theodolites used. This value also implies a good level of precision, i.e. 10% of the gauge volume width or better, laying perfectly within the required accuracy for neutron diffraction stress investigations.

4.3. Accuracy of entry curve analysis software

The accuracy of the entry curve analysis software in determining sample surface positions was calculated from the difference of the dimensions measured by wall scans and by CMM, which is presented in Table 6. The software packages implemented on each participating instrument were proven to be able to determine the positions of flat surfaces, that are perpendicular to the beam propagation plane (χ = 0°), to an accuracy better than 10% of the gauge volume width (Table 6 No. 1–5). The results were averaged over measurements taken at different detector angular positions, beam incident wavelengths and measurement geometries, where no significant variation was observed between the different setups. For flat surfaces that are not perpendicular with the beam propagation plane (inclined), the accuracy of the software analysis is strongly dependent on the gauge volume height used in the measurements. Using a gauge volume height of 2 mm, measurement on walls with tilt angle of χ = 2° and 10° can still be accurately determined to better than 5% of gauge volume width (Table 6 No. 6–7). With a larger gauge volume height, such as with the 10 mm investigations, the results indicate that for a flat surface inclined at χ = 2°, the attained accuracy was still within the 10% gauge volume width criterion (Table 6 No. 8). However, at tilt angles χ > 10° the determined accuracy with this gauge volume height becomes excessive, being larger than 20% of the gauge volume width (Table 6 No. 9).

Determination of horizontally curved surfaces with radius = 50 mm, perpendicular to the horizontal diffraction plane, i.e. the Tube with axis vertical, using the software packages implemented on each participating instrument mostly failed to determine the wall thicknesses to within the 10% of the gauge volume width criterion (see entries in Table 6). Values ranged from 10% to 17%. This became much worse, larger than 60% for the measurements offset 30 mm from the radial line. Analyses using a geometric model that accounts for the non-flat horizontal geometry such as "FIT Pseudo Strain" (T. Pirling, personal communication, September 2019), was able to determine the wall thickness within the 10% of the gauge volume width criterion (Table 6 No. 10) and will be applied in the other participating software

Table 5
Standard deviation of the offsets in the measurement of the 5-wall sample, indicative of the sample alignment precisions attained using the optical alignment systems.

Inst.	No	$hkl/2\theta_{det}$ (°)	NGV size (mm^3)	Measurement geometry	Std. deviation of offset (mm)
1	1	Fe(220)/83.6	0.6 × 0.6 × 2.0	Transmission	0.05
	2	Fe(311)/98.0	2.0 × 2.0 × 2.0	Reflection	0.10
2	3	Fe(220)/83	1.0 × 1.0 × 10.0	Transmission	0.10
	4			Reflection	0.12
	5	Fe(311)/102		Transmission	0.05
	6			Reflection	0.08
	7	Fe(311)/77.5		Transmission	0.03
3	8	Fe(220)/80	1.0 × 1.0 × 10.0	Transmission	0.10
	9			Reflection	0.09
	10	Fe(200)/55		Transmission	0.09
	11			Reflection	0.10
4	12	Multiple/90, −90	2.0 × 2.0 × 10.0	Transmission	0.05
	13			Reflection	0.05
	14		1.0 × 1.0 × 15.0	Transmission	0.05
	15			Reflection	0.09

Table 6
Average differences between wall scans and CMM results, representing the accuracy of the entry curve analysis software for different sample shapes.

Features	No	NGV size (mm^3)	Details	Average differences (mm)
Flat	1	0.6 × 0.6 × 2.0	χ = 0°	0.04
	2	1.0 × 1.0 × 8.0		0.05
	3	1.0 × 1.0 × 10.0		0.07
	4	1.0 × 1.0 × 15.0		0.05
	5	2.0 × 2.0 × 10.0		0.13
	6	1.0 × 1.0 × 2.0	χ = 2°	0.02
	7		χ = 10°	0.04
	8	1.0 × 1.0 × 10.0	χ = 2°	0.05
	9		χ = 10°	0.21
Curved, R= 50 mm, axis vertical, radial line	10	0.6 × 0.6 × 2.0	With geometric model	0.06
	11	1.0 × 1.0 × 2.0		0.17
	12	1.0 × 1.0 × 10.0	Without geometric model	0.13
	13	2.0 × 2.0 × 10.0		0.10
Curved, R = 50 mm, axis vertical, offset = 30 mm	14	1.0 × 1.0 × 2.0	Without geometric model	0.69
	15	1.0 × 1.0 × 15.0		0.63
Curved, R =50 mm, axis horizontal, radial line	16	1.0 × 1.0 × 2.0	Without geometric model	0.10
	17	1.0 × 1.0 × 10.0		0.05

tools. Results from assessing a vertically curved surface with radius = 50 mm, i.e. Tube with the axis horizontal, indicates that the modelling function applicable to flat surfaces, renders adequate accuracy for the wall thickness determination within the 10% of the gauge volume width criterion (Table 6 No. 16–17). This is because the corresponding surface can be considered flat in the horizontal direction while the curvature in the vertical is symmetrical, therefore the intensity curve effectively being similar to that of a flat surface. This situation though will not be attainable when the analysis is done offset from the diameter radial, i.e. any offset line.

5. Conclusion

The development of a harmonised approach for quantifying positional accuracy of setups in neutron strain scanners and benchmarking of instruments have been reported. The main take away points from this work are:

1. A set of samples and protocols have been demonstrated as verification tests for neutron strain scanners. Pin scans render a relatively simple exercise to evaluate the displacement of reference point as a function of detector angular position, while the foil scans exercise can provide a detailed assessment of the reference point relative to ω-rotation axis with accuracies up to 3% of the gauge volume width.
2. Wall scan results demonstrated that the method of scanning multiple flat surfaces with the neutron beam can be used to evaluate the effective precision of external sample alignment optical systems (in principle mechanical techniques such as touch probes would also suffice). Comparing sample thicknesses measured with neutron wall scans compared to CMM results, provided insight about the accuracy and robustness of the entry curve analysis software.
3. Benchmarking results showed that the positional accuracy of 10% of the gauge volume width (both instrument and sample alignment) can readily be attained. This agrees with the values reported in the VAMAS TWA20 report and are also within the limits recommended by ISO 21432:2019.
4. The investigations clearly demonstrated that reference point positions become displaced when the detector angular position is changed (may be required for multi-peak/multi-phase sample investigations with different $2\theta_{det}$ settings), therefore it becomes essential, that instrument re-alignments be performed at each specific detector position. In this case, it is also important to note that d_0 reference measurements have to be performed for each detector position. The alternative is to characterise the reference point displacement as a function of detector angular position, and correct for this.
5. Re-alignment at each specific detector position is especially important for measurements using radial collimator for diffracted

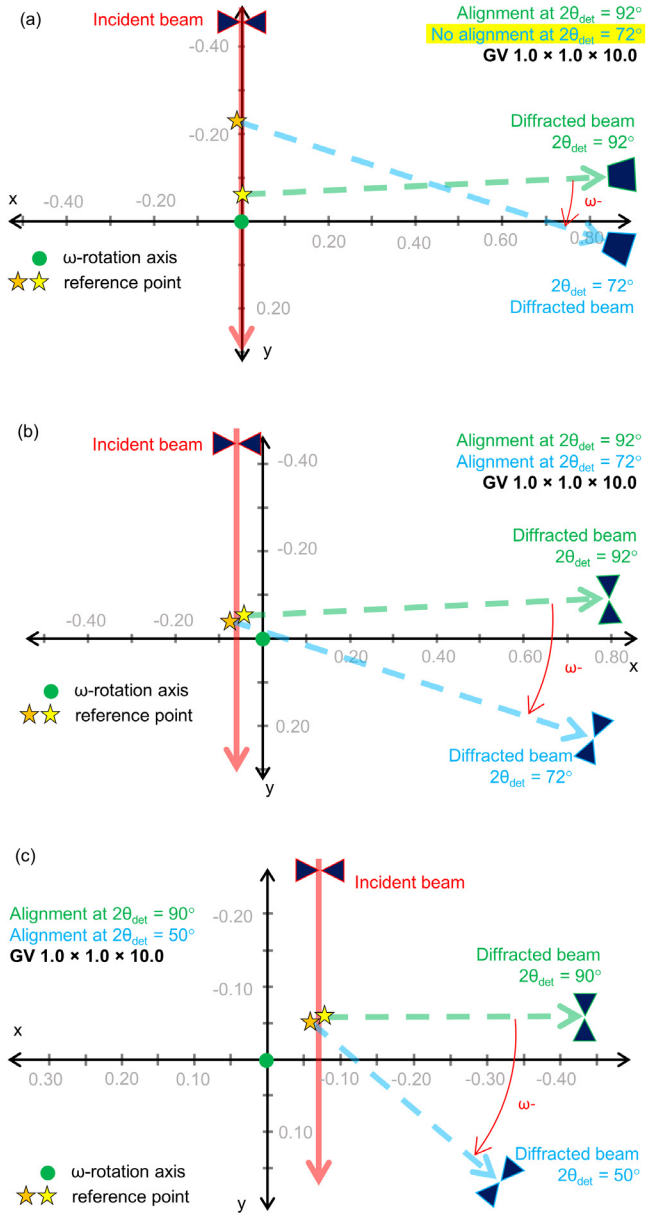

Fig. 10. Reference point relative to the centre of ω-rotation on Instruments 2 and 3, scales in mm. (a) Changing the detector angular position from 92° to 72° without following it up by diffracted beam-defining optics re-alignment shifted the reference point by around 200 μm; (b), (c) By performing re-alignment on each detector angular position, the reference point position is reproducible within 50 μm.

beam-defining optics, since the change in detector angular position should not have required re-alignment to preserve the lateral definition of the gauge volume if not due to the proposed rotation axes non-concentricity and/or mechanical contributions. Using slits, in contrast, re-alignment at each specific detector position is inherently needed to ensure the scattering angle is equal to the detector angle, i.e., to preserve the gauge volume definition, and therefore is already the common practice in neutron strain scanners utilising slits. Nevertheless, with proper alignment, results showed that the use of slits vs. collimators provides similar accuracies in reference point positioning.

6. For cases where a very accurate sample positioning is required, entry scans are preferred. In simple cases, i.e. flat surfaces perpendicular to the beam plane, accuracies better than 10% of gauge volume width can be achieved. For more complicated features, like inclined or curved surfaces, the gauge volume height and the inclusion of appropriate geometric modelling largely influence the accuracy of the surface determination.
7. Results from the current work can be translated into positional accuracies that can realistically be expected during a comprehensive residual stress characterisation on the instruments. For measurement of buried structures such as welds, which are likely to rely on the optical sample alignment system, positional accuracy ranging from 100 to 400 μm can be expected, dependent of the size of the gauge volume. For measurement of near surface stresses (e.g., surface treatments, coatings, etc.), high stress gradients, or any other cases requiring higher accuracy, sub-100 μm positional accuracy can be achieved through entry-scan methods, albeit at a slight penalty of longer measurement time.

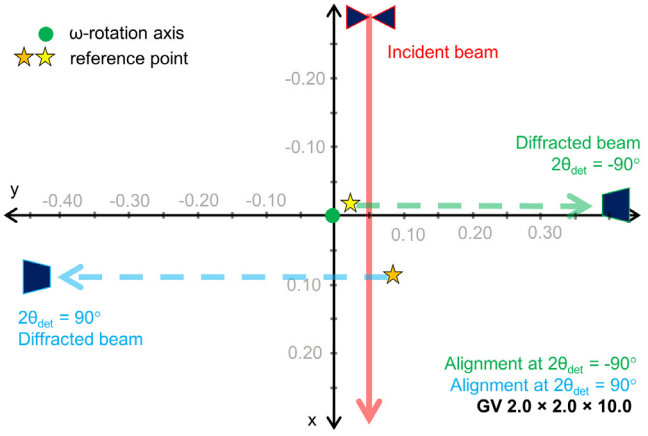

Fig. 11. Reference point relative to the centre of ω-rotation on Instrument 4, scales in mm. The results indicate that the two detector banks are misaligned 30-120 μm from the centre of ω-rotation and ~100 μm with each other (~5% of gauge volume).

This work has laid the groundwork for the characterisation of neutron strain scanners using a common protocol. The protocol should be constantly updated and improved and, from the lesson learned during the project, there is some scope for future work. These include more comprehensive characterisation of reference point position as a function of detector angular positions, characterisation of gauge volume shape for different setups, evaluation on the influence of the gauge volume height on the accuracy of entry scans for surface and/or interface determination, and improvement of geometric models for the entry curve analysis software applicable to non-flat surfaces and/or to complex geometries.

We invite other neutron strain scanners to perform a similar exercise of calibration & alignment measurements and adopt them as in present protocol. A set of sister samples has been made available as a major step in acquiring the Neutron Quality Label, and more importantly to improve the overall quality and repeatability of neutron diffraction as a method for stress determination.

CRediT authorship contribution statement

R.S. Ramadhan: Methodology, Investigation, Formal analysis, Writing - original draft, Visualization. **S. Cabeza:** Conceptualization, Methodology, Investigation, Writing - review & editing, Project administration. **T. Pirling:** Conceptualization, Methodology, Investigation, Software. **S. Kabra:** Conceptualization, Methodology, Investigation. **M. Hofmann:** Conceptualization, Methodology, Investigation, Writing - review & editing. **J. Rebelo Kornmeier:** Investigation, Writing - review & editing. **A.M. Venter:** Conceptualization, Methodology, Investigation, Writing - review & editing. **D. Marais:** Investigation, Formal analysis, Software, Writing - review & editing.

Declaration of competing interest

The authors declare that they have no known competing financial interests or personal relationships that could have appeared to influence the work reported in this paper.

Acknowledgements

This project is carried out as a part of BrightnESS^2. BrightnESS^2 is funded by the European Union Framework Programme for Research and Innovation Horizon 2020, under grant agreement 823867. The authors are grateful for the provision of beam time at the participating facilities: ENGIN-X, ISIS (RB2030003), MPISI, Necsa (2019/12/20-6201), SALSA, ILL (10.5291/ILL-DATA.INTER-468) and STRESS-SPEC, MLZ (16405). The authors would like to thank S. MARTINEZ GARCIA of Institut Laue-Langevin for the support in sample fabrication and CMM measurements.

References

[1] G.A. Webster, A.N. Ezeilo, Neutron scattering in engineering applications, Phys. B Condens. Matter. 234–236 (1997) 949–955, http://dx.doi.org/10.1016/S0921-4526(96)01221-5.

[2] S. Pierret, T. Etter, A. Evans, H. Van Swygenhoven, Origin of localized rafting in Ni-based single crystal turbine blades before service and its influence on the mechanical properties, Acta Mater. 61 (2013) 1478–1488, http://dx.doi.org/10.1016/j.actamat.2012.11.024.

[3] L. Edwards, M.E. Fitzpatrick, P.E. Irving, I. Sinclair, X. Zhang, D. Yapp, An integrated approach to the determination and consequences of residual stress on the fatigue performance of welded aircraft structures, J. ASTM Int. 3 (2006) 1–17, http://dx.doi.org/10.1520/stp45330s.

[4] M. Preuss, P.J. Withers, G.J. Baxter, A comparison of inertia friction welds in three nickel base superalloys, Mater. Sci. Eng. A 437 (2006) 38–45, http://dx.doi.org/10.1016/j.msea.2006.04.058.

[5] P.J. Bouchard, D. George, J.R. Santisteban, G. Bruno, M. Dutta, L. Edwards, E. Kingston, D.J. Smith, Measurement of the residual stresses in a stainless steel pipe girth weld containing long and short repairs, Int. J. Press. Vessels Pip. 82 (2005) 299–310, http://dx.doi.org/10.1016/j.ijpvp.2004.08.008.

[6] A. Narayanan, M. Mostafavi, T. Pirling, S. Kabra, R. Lewis, M.J. Pavier, M.J. Peel, Residual stress in laser cladded rail, Tribol. Int. 140 (2019) 105844, http://dx.doi.org/10.1016/j.triboint.2019.105844.

[7] R. Pan, T. Pirling, J. Zheng, J. Lin, C.M. Davies, Quantification of thermal residual stresses relaxation in AA7xxx aluminium alloy through cold rolling, J. Mater. Process. Technol. 264 (2019) 454–468, http://dx.doi.org/10.1016/j.jmatprotec.2018.09.034.

[8] F. Foadian, A. Carradó, H.G. Brokmeier, W.M. Gan, N. Schell, N. Al-Hamdany, H. Palkowski, Evolution of texture in precision seamless tubes investigated by synchrotron and neutron radiation measurement, Mater. Charact. 151 (2019) 582–589, http://dx.doi.org/10.1016/j.matchar.2019.03.041.

[9] J.S. Robinson, C.E. Truman, A. O'Donovan, J. Rebelo Kornmeier, Uphill quenching to reduce residual stress in a heat treatable aluminium alloy, Mater. Sci. Technol. 35 (2019) 1864–1871, http://dx.doi.org/10.1080/02670836.2019.1651986.

[10] G.A. Webster, Neutron diffraction measurements of residual stress in a shrink-fit ring and plug VAMAS Report No. 38, London, National Physical Laboratory, 2000.

[11] A.G. Youtsos, C. Ohms, European standardization activities on residual stress analysis by neutron diffraction, Appl. Phys. (2002) http://dx.doi.org/10.1007/s003390201841.

[12] Non-destructive testing—Standard test method for determining residual stresses by neutron diffraction, Int. Organ. Stand. (2019).

[13] C. Carlile, C. Petrillo, M. Carpineti, M. Donzelli, Neutron Scattering Facilities in Europe - Present Status and Future Perspectives, Dipartimento di Fisica - Università degli Studi di Milano, Milan, 2016.

[14] Brightness, (n.d.). https://brightness.esss.se/ (Accessed April 3, 2020).

[15] R.S. Ramadhan, S. Cabeza, Pilot project for a neutron quality label for residual stress analysis: Development of a common calibration protocol, Grenoble (2020).

[16] P.C. Brand, H.J. Prask, New methods for the alignment of instrumentation for residual-stress measurements by means of neutron diffraction, J. Appl. Crystallogr. 27 (1994) 164–176, http://dx.doi.org/10.1107/S0021889893007605.

[17] T. Pirling, G. Bruno, P.J. Withers, SALSA-A new instrument for strain imaging in engineering materials and components, Mater. Sci. Eng. A 437 (2006) 139–144, http://dx.doi.org/10.1016/j.msea.2006.04.083.

[18] M. Hofmann, W. Gan, J. Rebelo-Kornmeier, STRESS-SPEC: Materials science diffractometer, J. Large-Scale Res. Facil. 1 (2015) 1–25.

[19] A.M. Venter, P.R. van Heerden, D. Marais, J.C. Raaths, MPISI: The neutron strain scanner materials probe for internal strain investigations at the SAFARI-1 research reactor, Phys. B Condens. Matter. 551 (2018) 417–421, http://dx.doi.org/10.1016/j.physb.2017.12.011.

[20] J.R. Santisteban, M.R. Daymond, J.A. James, L. Edwards, ENGIN-X: A third-generation neutron strain scanner, J. Appl. Crystallogr. 39 (2006) 812–825, http://dx.doi.org/10.1107/S0021889806042245.

[21] GeoGebra, (n.d.). https://www.geogebra.org/?lang=en (Accessed May 18, 2020).

[22] D. Marais, A.M. Venter, J. Markgraaff, Data processing at the South African Nuclear Energy Corporation SOC Ltd(Necsa) neutron diffraction facility, in: Proceeding of SAIP2015, 2016, pp. 143–148.

[23] T. Pirling, D.J. Hughes, J.S. Robinson, Precise determination of residual stresses in large specimens by neutron diffraction, in: Mech. Stress Eval. By Neutrons Synchrotron Radiat, Trans Tech Publications Ltd, 2010, pp. 80–85, http://dx.doi.org/10.4028/www.scientific.net/MSF.652.80.